Ion-induced Assemblies of Highly Anisotropic Nanoparticles Are Governed by Ion-ion Correlation and Specific Ion Effects

*Tobias Benselfelt[1, 2, *], Malin Nordenström[1, 2], Mahiar Max Hamedi[1,2], and Lars Wågberg[1, 2, *]*

[1]Department of Fibre and Polymer Technology, Wallenberg Wood Science Center, KTH Royal Institute of Technology, Teknikringen 56-58, 10044, Stockholm, Sweden.

[2]Department of Fibre and Polymer Technology, Division of Fibre Technology, KTH Royal Institute of Technology, Teknikringen 56-58, 10044, Stockholm, Sweden.

[*]Corresponding authors: wagberg@kth.se, bense@kth.se

Contents

Experimental section

Materials

Unless otherwise is stated, CNFs were prepared from a never-dried dissolving sulfite pulp that was kindly provided by Aditya Birla Domsjö Fabriker AB. The pulp had a hemicellulose content of 4-5 % and a lignin content of 0-1 %.[1] The chloride salts of sodium(I), lithium(I), potassium(I), cesium(I), barium(II), calcium(II), magnesium(II), manganese(II), zinc(II), copper(II), aluminum(III), and iron(III), as well as acetic acid, dibasic sodium phosphate, citric acid, TEMPO (2,2,6,6-Tetramethyl-1-piperidinyloxy), sodium chlorite, and sodium hypochlorite (14 vol%) were purchased from Sigma Aldrich. Durapore membrane filters (DVPP09050 or VVLP09050, pore size 0.65 or 0.1 μm) were purchased from Merck, Sweden. Montmorillonite clay (MMT) was purchased from BYK Instruments in Germany with the product name Cloisite Na+.

Preparation of CNF and MMT dispersions

Medium- and high-charge-density anionic CNF dispersions were prepared by TEMPO-mediated oxidation according to the protocol established by Saito et al.[2] The pulp was first purified with $NaClO_2$ (0.3 wt%) in acetate buffer (0.1 M, pH 4.6) at 60°C for 1h. After purification, the pulp (15 g dry weight) was suspended in a phosphate buffer (0.05 M, pH 6.8, 1350 mL, 60°C), followed by the addition of $NaClO_2$ (150 mmol), TEMPO (1.5 mmol) and NaClO (15 mmol, diluted in 150 mL phosphate buffer). The reaction proceeded for 140 min (medium charge CNFs) or 72 h (high charge CNFs) under continuous stirring. Following the oxidation, the pulp was washed with deionized water using vacuum filtration and diluted to 1.5-2 wt%. The CNFs were liberated mechanically in a high-pressure homogenizer (Microfluidizer M-110EH, Microfluidics Corp., USA), by passing the suspension once through two large chambers (400 and 200 μm) and four times through two small chambers (200 and 100 μm).

Cationic CNFs with high charge density were prepared by a procedure established by Pei et al.[3] Details regarding the chemicals and the pulp used are found in the cited publication. Cationic CNFs with low charge density were prepared with the same procedure and were kindly provided by Innventia AB now RISE Bioeconomy.[4]

In order to obtain colloidally stable dispersions, the 1.5-2 wt% CNF gel was diluted to 0.15 wt% followed by probe sonication (10 min, 30 % amplitude, 6 mm microtip probe) and centrifugation (1h, 4100 g). The supernatant fraction was kept while the aggregated pellet was discarded. The surface charge density, measured by polyelectrolyte titration (Stabino, Particle Metrix GmbH, Germany), was determined to be 0.64 mmol/g and 1.2 mmol/g for the anionic CNFs (medium and high charge), and 0.36 mmol/g and 1.2 mmol/g for the cationic CNFs (low and high charge).

The MMT suspension was prepared by dispersing 10 g in 2 L of Milli-Q water using an Ultra-Turrax apparatus at 15000 rpm for 30 min. The suspension was then sonicated (5 min, 70 % amplitude, 12 mm probe) and centrifuged (30 min, 4100 g). Sonication/centrifugation was repeated until there were no more visible residues, typically three times. The final solid content of the clay suspension was 0.3 wt%.

Preparation of CNF and MMT films

CNF and clay films were prepared by vacuum filtration using a microfiltration assembly from Kontes. For the medium charge anionic CNFs and both cationic CNFs, 0.65 μm Durapore filters were used, and for the high charge anionic CNFs and MMT clay, 0.1 μm Durapore filters were used. Dispersions containing 0.1-0.15 wt% CNFs or clay were filtered overnight to produce films with a diameter of 8

cm, a dry weight of 200-400 mg and a dry thickness of 30-60 µm. For all CNFs, the filter cake (about 90 % water) was dried for 15-20 minutes using a Rapid Köthen sheet former (Paper Testing Instruments, Austria) at a reduced pressure of 95 kPa and a temperature of 93 °C for the anionic CNFs, and at 50 °C for the cationic CNFs, due their sensitivity to heat. For clay, the filter cake (about 85% water) was solvent-exchanged in isopropanol for a few hours before drying at 93 °C for 15 minutes.

Measuring the degree of swelling of CNF and MMT films

The swelling of polyelectrolytes gels can be described by three pressures according to Flory:[5]

$$|\Pi_{net}| = |\Pi_{mix}| + |\Pi_{ion}| \qquad (S1)$$

where Π_{mix} is the pressure based on the thermodynamics of mixing the polyelectrolytes in the gel with water, Π_{net} is the network pressure of the gel working as an opposite force, and Π_{ion} is the osmotic pressure associated with the charged groups in the gel. This equation can also represent the swelling of a CNF/MMT film, and this means that the swelling provides information about the interactions in the CNF/MMT network (Π_{net}) if the mixing- (Π_{mix}) and the ionic pressure (Π_{ion}) are assumed to be constant at a given valency of the counter-ions. The degree of swelling in the presence of different counter-ions provides information about whether the attractive interactions in the CNF/MMT film are caused by ion-ion correlation, specific ion effects, or something else.

The swelling was measured as the relative thickness change according to:

$$Swelling = \frac{d_{wet} - d_{dry}}{d_{dry}} \qquad (S2)$$

where d is the thickness of the film. This approach can be used since CNF films have a unidirectional swelling at moderate degrees of swelling and therefore follow the same trend as the mass swelling.[6]

The dry films were soaked in 1 wt% salt solutions for 24 hours to exchange the counter-ions and then equilibrated against Milli-Q water for 24 hours by changing the water twice. This procedure is illustrated in Figure 2. The thickness was measured with a thickness gauge and a microscope cover glass was used for the wet samples to spread the load so that they were not damaged by pressure from the gauge pin.

FTIR

Fourier transformed infrared spectroscopy (FTIR) was used to study the vibrational change of the asymmetric (1600 cm^{-1}) and symmetric (1400 cm^{-1}) vibrations of carboxylic acids in the presence of different counter-ions. A Perkin-Elmer Spectrometer 100 with a Graseby Specac LTD Golden attenuated total reflectance (ATR) gate was used at ambient conditions.

The surface charge density of the anionic CNFs

The widths of the anionic CNFs were determined using atomic force microscopy (AFM) height measurements. The samples were prepared by adsorption of polyethyleneimine (0.1 gL^{-1}, 15 s) onto

freshly cleaved mica, followed by adsorption of CNF (0.005 wt%, 15 s). After each adsorption step the samples were rinsed with Milli-Q water. Images were acquired with a MultiMode 8 AFM (Bruker, USA) in the ScanAsyst mode in air, using a cantilever with a 70 kHz resonance frequency, 0.4 Nm^{-1} spring constant and 2 nm tip radius (ScanAsyst-Air, Bruker, USA). The widths were determined by height measurements of 100 fibrils and were measured to be 2.95 ± 0.15 nm and 3.11 ± 0.14 nm for medium- and high-charge CNFs respectively.

The surface charge density was calculated to be 0.07 C/m^2 for medium-charge CNFs and 0.13 C/m^2 for high-charge CNFs, by assuming that the fibrils had a square cross-section.

Measuring the mechanical properties of CNF films in the wet state

Dry CNF films were cut into 3 x 50 mm samples and where treated with metal ions in the same way as for the swelling measurements. The samples were picked up from the water and the surfaces were dried with a tissue. The samples were tested in an Instron 5944 (500 N load cell) with a gauge length of 20 mm and a strain rate of 2 mm/min. Presented stress-strain curves are the most representative of 5 samples.

Theory

Ion-ion correlation

The theory of ion-ion correlation was pioneered by Oosawa[7] in the 1970s and was further developed during the 1980s by Wennerström and Kjellander and co-workers.[8, 9, 10]

The mean field approximation of the Poisson-Boltzmann equation in the Debye-Hückel theory, which is the foundation for the double-layer repulsion in the DLVO theory, assumes that the ions are dimensionless point charges that are evenly distributed outside a charged surface.[11] In reality, the counter-ion cloud fluctuates due to thermal energy or the influence of surrounding electrical fields. These fluctuations lead to a polarization of the counter-ion cloud and the local potential variations in the counter-ion cloud of macro-ions, i.e. polyelectrolytes or charged colloidal particles, in proximity can start to correlate leading to the induction of an attractive electrostatic interaction between the macro-ions. An analogy can easily be made to London dispersion interactions in the van der Waals theory but with a correlated movement of ions instead of electrons. A simpler nomenclature to separate these interactions could be 'electron dispersion interactions' and 'ion dispersion interactions', but in the present work dispersion interactions refer only to electron dispersion. The fluctuations can also lead to a contraction of the counter-ion clouds, which reduces the double-layer overlap, and thus the double-layer repulsion at a given separation.[8]

As a consequence, the DLVO theory fails for more complex systems that deviate from the basic assumptions in the Poisson-Boltzmann equation and the Debye-Hückel theory. For monovalent counter-ions outside surfaces with low charge density, the ion cloud fluctuations are small and often compensated for by ion core-core repulsion,[12] and the mean-field approximation is then surprisingly accurate. However, at higher surface charge densities and with multivalent counter-ions, the ion-ion correlation becomes significant. The magnitude of the ion-ion correlation, for multivalent counter-ions, can in highly charged systems and at small separations overpower the double-layer repulsion, and this results in an overall attraction where the DLVO theory predicts repulsion.

The strength of the ion-ion correlation interactions is, according to the suggested theories, influenced by several parameters that are still under investigation, but some of the discussed criteria are as follows:

- High aspect ratio macro-ions lead to greater ion cloud fluctuations.[7]
- Ion-ion interactions lead to a stronger correlation.[13]
- Higher valency of the counter-ions leads to a more polarizable ion cloud and hence stronger ion-ion correlation.[7, 8, 14]
- A higher surface charge density and higher volume concentration of the macro-ion lead to stronger ion-ion correlation.[8, 13] For example, dilute dispersions of CNFs can be colloidally stable even with multivalent counter-ions, at least for short periods of time.[15]
- Large counter-ions lead to core-core repulsion that diminishes the ion-ion correlation. This effect can be neglected if the counter ion radius is much smaller than the Bjerrum length (0.7 nm), which is true for most cationic counter-ions.[14]

Specific ion effects and the Hofmeister series

The term "specific ion effects" is a compilation of observed colloidal behaviors due to non-electrostatic interactions on the atomic/molecular scale that are not considered in the DLVO theory, for example adsorption of ions to surfaces mediated by dispersion interactions.[16, 17, 18] The specific ion effects were first investigated by Hofmeister as early as 1888 and this led to several studies on how

different salts affected the state of proteins in solution, which later resulted in the famous Hofmeister series.[19] Specific ion effects are still being intensely discussed in the scientific literature and there is as yet no universal theory on the subject.[16]

The specific ion effects describe how colloidal systems deviate from the basic assumptions in the Debye-Hückel approximation when, for example, the polarizability of the ions and solvent interactions, such as hydration, are taken into consideration at an atomic level. This leads to several proposed interaction mechanisms such as:

- Ion-ion dispersion interactions.[18, 20, 21] (also affect ion-ion correlation).
- Ion-macro-ion dispersion interactions,[18] which lead to a reduced effective surface charge.
- Ion-macro-ion dative-covalent interactions; also known as metal-ligand complexes or coordination complexes (further described in the following section).
- Hydration, i.e. ion-water or macro-ion-water, interactions. This is important for all the above mechanisms but also influence how ions are included in or excluded from the hydration layer at an interface.[18]

The specific ion effects, except metal-ligand complexes, are probably easiest to observe in the presence of monovalent counter-ions where the ion-ion correlation interactions are weak. Anionic counter-ions are generally more polarizable and hence are involved in greater dispersion interactions, and this is probably why uncharged surfaces become slightly negative when placed in an electrolyte solution due to the adsorption of anions.[18]

Metal-ligand complexes: a well characterized specific ion effect

Multivalent metal cations can coordinate with electron donating ligands in water to form metal-ligand complexes and this should be considered a specific ion effect even though it may be referred to as an ion-head-group interaction in these discussions.[16, 22]

The general trends when it comes to the stability of complexes with divalent cations were summarized by Irving and Williams in the early 1950s.[23, 24] Today, the complex stability is best described by the combination of the following theories:

- The size of the ion indicates how strongly the nucleus attracts electrons. As a consequence, small ions are more ready to bind electron-donating ligands, while larger ions are more stable and gain less energy by forming complexes. [22, 25]
- The lowest energy state for each atom is to have an electron configuration similar to that of the closest noble gas. The alkaline earth metal ions and aluminum ions are however already in a noble gas configuration and are less likely to form complexes, unlike the transition metals that can lower their free energy by filling the d-orbitals. They do so by forming hybrid orbitals to share electrons with ligands in dative covalent bonds.[25]
- The ligand field theory describes how the energy levels of the d-orbitals are affected by the geometry of the formed complex. The d-orbitals are split into low and high energy levels and the complex can minimize its energy by placing electrons in the low energy states. The split of the energy levels of the d-orbital is known as field splitting and depends on the properties of the ligand. Photons with an energy that matches the field split energy can excite electrons and this leads to the distinct colors of certain complexes.[26]
- The chelate effect is the entropic gain when two or more ligands are covalently linked, and this reduces the free energy compared to that of the complex with independent ligands.[22]

- Steric/crowding effects arise from the repulsion between ligands or between ligand and water associated to the ion. This effect is greater for small ions in combination with bulkier ligands and this sometimes appears as a deviation from the expected complex stability.[23, 24, 27, 28]

According to the above theory, multivalent metal ions can form complexes with ligands on the surface of nanoparticles in either inter- or intra complexes.[29] Intra-complexes create a net zero surface charge while inter-complexes supposedly act as crosslinkers. The hypothetical formation of inter-complexes (crosslinks) should be sensitive to the ratio of the ligand and to metal ion and this has been shown for catechol-iron complexes.[30]

Theoretical calculations

Calculating the effective polarizability

The effective polarizabilities in water of the multivalent cations were calculated according to Ninham.[20] The effective polarizabilities of the anionic and monovalent counter-ions were taken directly from Ninham. For simplicity we decided to use the radius of the multivalent cationic ions with six coordinated water molecules (Shannon radius) to calculate the polarizabilities for the multivalent ions.[31] This may not be the most accurate approach, but the small differences with respect to the accuracy of the experimental data in this work, should not affect the conclusions.

The effective (in water) polarizability (α^*) is calculated according to:[20, 21]

$$\alpha^* = \frac{3V_i[\varepsilon_i - \varepsilon_m]}{4\pi[\varepsilon_i + 2\varepsilon_m]} \quad \text{(S3)}$$

where V_i is the volume of the ion, ε_i is the dielectric constant of the ion, and ε_m is the dielectric constant of water, which is 80. The dielectric constant of the ion is calculated according to:

$$\varepsilon_i = 1 + 4\pi\frac{\alpha_i}{V_i} \quad \text{(S4)}$$

where α_i is the intrinsic or vacuum polarizability of the ion. The parameter values used for the calculations are given in Table S3. Table S4 shows the calculated effective polarizabilities using the Shannon radius compared to a hard sphere ionic radius for multivalent ions. Table S5 shows the effective hard sphere radius and effective polarizabilities for monovalent and anionic ions calculated by Ninham and co-workers.[20]

Tables

Table S1. Swelling ± 95% confidence interval ($n = 3$) for the films prepared from anionic CNFs of medium charge (0.64 mmol/g) and high charge (1.2 mmol/g) in the presence of different counter-ions. The values for MMT clay are the average of two measurements with an accuracy similar to that of the high charge CNF samples.

	Swelling (μm/μm)											
	Li^+	**Na^+**	**K^+**	**Cs^+**	**Ba^{2+}**	**Ca^{2+}**	**Mg^{2+}**	**Mn^{2+}**	**Zn^{2+}**	**Cu^{2+}**	**Al^{3+}**	**Fe^{3+}**
Medium charge	14.1 ± 1.5	13.6 ± 0.4	11.4 ± 1.0	9.3 ± 0.4	3.3 ± 0.6	3.5 ± 0.8	4.1 ± 0.3	3.6 ± 0.2	3.3 ± 0.2	2.7 ± 0.6	2.3 ± 0.2	2.0 ± 0.2
High charge	68 ± 8	55 ± 7	52 ± 5	43 ± 4	3.6 ± 0.1	4.0 ± 0.1	4.7 ± 0.1	4.1 ± 0.2	3.7 ± 0.0	3.1 ± 0.3	2.5 ± 0.1	2.1 ± 0.0
MMT clay	-	Dissolves	-	-	1.7	2.4	2.8	3.0	2.6	2.7	1.1	1.0

Table S2. Swelling ± 95% confidence interval ($n = 3$) for the films prepared from cationic CNFs of high (1.2 mmol/g) and low (0.36 mmol/g) charge in the presence of different counter-ions.

	Swelling (μm/μm)			
	$Acetate^-$	**Cl^-**	**$Phosphate^{3-}$**	**$Citrate^{3-}$**
Cationic low charge	31.6 ± 0.7	24.1 ± 0.5	6.8 ± 0.1	4.6 ± 0.1
Cationic high charge	551 ± 39[a]	452 ± 16	93.4 ± 2.7	10.4 ± 0.5

a. dissolved over time

Table S3. Parameter values for the different multivalent ions

		Ba^{2+}	**Ca^{2+}**	**Mg^{2+}**	**Mn^{2+}**	**Zn^{2+}**	**Cu^{2+}**	**Al^{3+}**	**Fe^{3+}**
Ionic radius (Å) including 6 H_2O[31]		1.35	1.00	0.720	0.830	0.740	0.730	0.535	0.645
Intrinsic polarizability (Å^3)[32, 33, 34, 35]	**Ref 32**	1.56	0.49	0.075		0.420			
	Ref 33				0.618	0.428			0.259
	Ref 34	1.55 1.68	0.51 0.47	0.012 0.12 0.094				0.052 0.065 0.067	
	Ref 35		0.47						0.247
	Average	1.60	0.49	0.075	0.618	0.424	-	0.061	0.253

Table S4. Calculated effective polarizability in water (Å^3) of the different multivalent ions

	Ba^{2+}	**Ca^{2+}**	**Mg^{2+}**	**Mn^{2+}**	**Zn^{2+}**	**Cu^{2+}**	**Al^{3+}**	**Fe^{3+}**
Ninham with hard sphere radius	-1,11	-0,32	-0,08					
Our calculations	-1.16	-0,48	-0,18	-0,26	-0,19	-	-0,076	-0,12

Table S5. Ionic hard sphere radius and effective polarizability in water (Å^3) of monovalent cationic ions and anionic ions according to Ninham.[20]

	Li^+	Na^+	K^+	Cs^+	$Acetate^-$	Cl^-	$Phosphate^{3-}$	$Citrate^{3-}$
Ionic hard sphere radius (Å)[21]	0.42	0.67	1.06	1.62	2.41	1.86	2.64	3.32
Effective polarizability (Å^3)[20]	-0.04	-0.14	-0.55	-2.01	-1.35	-3.03	-8.47	-17.31

Figures

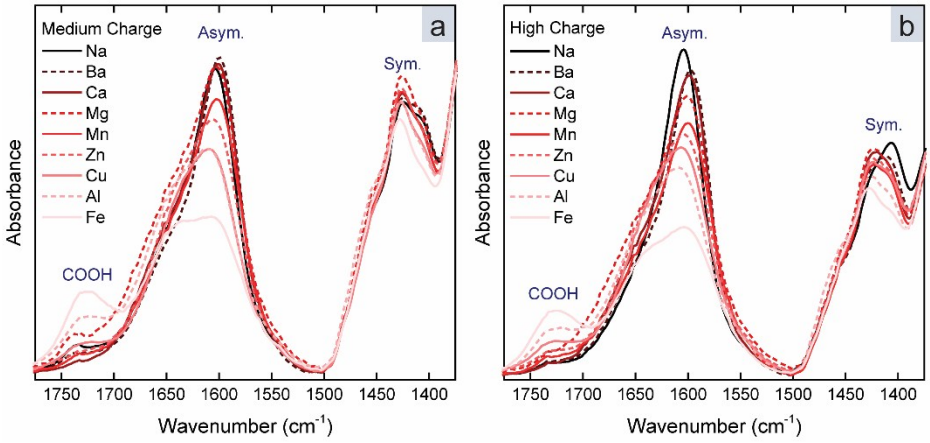

Figure S1. FTIR spectra of dried CNF films treated with different counter-ions. a) Medium charge CNFs. b) High charge CNFs.

References

1. Wågberg, L.; Decher, G.; Norgren, M.; Lindström, T.; Ankerfors, M.; Axnäs, K. The Build-Up of Polyelectrolyte Multilayers of Microfibrillated Cellulose and Cationic Polyelectrolytes. *Langmuir* **2008,** *24*, 784-795.
2. Saito, T.; Hirota, M.; Tamura, N.; Kimura, S.; Fukuzumi, H.; Heux, L.; Isogai, A. Individualization of Nano-Sized Plant Cellulose Fibrils by Direct Surface Carboxylation Using TEMPO Catalyst under Neutral Conditions. *Biomacromolecules* **2009,** *10*, 1992-1996.
3. Pei, A.; Butchosa, N.; Berglund, L. A.; Zhou, Q. Surface quaternized cellulose nanofibrils with high water absorbency and adsorption capacity for anionic dyes. *Soft Matter* **2013,** *9*, 2047-2055.
4. Ghanadpour, M.; Carosio, F.; Wågberg, L. Ultrastrong and flame-resistant freestanding films from nanocelluloses, self-assembled using a layer-by-layer approach. *Applied Materials Today* **2017,** *9*, 229-239.
5. Flory, P. J. *Principles of Polymer Chemistry*; Cornell University Press1953.
6. Benselfelt, T.; Engstrom, J.; Wagberg, L. Supramolecular Double Networks of Cellulose Nanofibrils and Algae Polysaccharides with Excellent Wet Mechanical Properties. *Green Chem.* **2018**.
7. Oosawa, F. Polyelectrolytes. In *Polyelectrolytes*; Marcel Dekker, 1971, pp 50-126.
8. Guldbrand, L.; Jönsson, B.; Wennerström, H.; Linse, P. Electrical double layer forces. A Monte Carlo study. *The Journal of Chemical Physics* **1984,** *80*, 2221-2228.
9. Kjellander, R.; Marčelja, S. Correlation and image charge effects in electric double layers. *Chem. Phys. Lett.* **1984,** *112*, 49-53.

10. Joensson, B.; Wennerstroem, H.; Halle, B. Ion distributions in lamellar liquid crystals. A comparison between results from Monte Carlo simulations and solutions of the Poisson-Boltzmann equation. *The Journal of Physical Chemistry* **1980,** *84*, 2179-2185.
11. Verwey, E. J. W.; Overbeek, J. T. G.; Overbeek, J. T. G. *Theory of the Stability of Lyophobic Colloids*; Dover Publications1999.
12. Kjellander, R.; Marcelja, S. Double-layer interaction in the primitive model and the corresponding Poisson-Boltzmann description. *The Journal of Physical Chemistry* **1986,** *90*, 1230-1232.
13. Evans, D. F.; Wennerström, H. *The Colloidal Domain: Where Physics, Chemistry, Biology, and Technology Meet*; 2nd ed.; Wiley-Vch, 1999.
14. Jönsson, B.; Wennerström, H. ION–ION CORRELATIONS IN LIQUID DISPERSIONS. *The Journal of Adhesion* **2004,** *80*, 339-364.
15. Sone, A.; Saito, T.; Isogai, A. Preparation of Aqueous Dispersions of TEMPO-Oxidized Cellulose Nanofibrils with Various Metal Counterions and Their Super Deodorant Performances. *ACS Macro Letters* **2016,** *5*, 1402-1405.
16. Kunz, W. Specific ion effects in colloidal and biological systems. *Current Opinion in Colloid & Interface Science* **2010,** *15*, 34-39.
17. Boström, M.; Williams, D. R. M.; Ninham, B. W. Specific Ion Effects: Why DLVO Theory Fails for Biology and Colloid Systems. *Phys. Rev. Lett.* **2001,** *87*, 168103.
18. Parsons, D. F.; Bostrom, M.; Nostro, P. L.; Ninham, B. W. Hofmeister effects: interplay of hydration, nonelectrostatic potentials, and ion size. *PCCP* **2011,** *13*, 12352-12367.
19. Hofmeister, F. Zur Lehre von der Wirkung der Salze. *Archiv für experimentelle Pathologie und Pharmakologie* **1888,** *25*, 1-30.
20. Ninham, B. W.; Nostro, P. L. *Molecular Forces and Self Assembly: In Colloid, Nano Sciences and Biology*; Cambridge University Press2010.
21. Parsons, D. F.; Ninham, B. W. Ab Initio Molar Volumes and Gaussian Radii. *The Journal of Physical Chemistry A* **2009,** *113*, 1141-1150.
22. House, J. E. Chapter 19 - Composition and Stability of Complexes. In *Inorganic Chemistry (Second Edition)*; Academic Press, 2013, pp 643-664.
23. Williams, R. J. P. 722. The stability of the complexes of the group IIA metal ions. *Journal of the Chemical Society (Resumed)* **1952**, 3770-3778.
24. Irving, H.; Williams, R. J. P. 637. The stability of transition-metal complexes. *Journal of the Chemical Society (Resumed)* **1953**, 3192-3210.
25. House, J. E. Chapter 16 - Introduction to Coordination Chemistry. In *Inorganic Chemistry (Second Edition)*; Academic Press, 2013, pp 553-590.
26. House, J. E. Chapter 17 - Ligand Fields and Molecular Orbitals. In *Inorganic Chemistry (Second Edition)*; Academic Press, 2013, pp 591-616.
27. Hancock, R. D.; Marsicano, F. Parametric Correlation of Formation Constants in Aqueous Solution. 2. Ligands with Large Donor Atoms. *Inorg. Chem.* **1980,** *19*, 2709-2714.
28. Hancock, R. D.; Marsicano, F. Parametric correlation of formation constants in aqueous solution. 1. Ligands with small donor atoms. *Inorg. Chem.* **1978,** *17*, 560-564.
29. Williams, K. S.; Andzelm, J. W.; Dong, H.; Snyder, J. F. DFT study of metal cation-induced hydrogelation of cellulose nanofibrils. *Cellulose* **2014,** *21*, 1091-1101.
30. Zeng, H.; Hwang, D. S.; Israelachvili, J. N.; Waite, J. H. Strong reversible Fe³⁺-mediated bridging between dopa-containing protein films in water. *Proceedings of the National Academy of Sciences* **2010,** *107*, 12850-12853.
31. Shannon, R. Revised effective ionic radii and systematic studies of interatomic distances in halides and chalcogenides. *Acta Crystallographica Section A* **1976,** *32*, 751-767.
32. Yu, H.; Whitfield, T. W.; Harder, E.; Lamoureux, G.; Vorobyov, I.; Anisimov, V. M.; MacKerell, A. D.; Roux, B. Simulating Monovalent and Divalent Ions in Aqueous Solution Using a Drude Polarizable Force Field. *J. Chem. Theory Comput.* **2010,** *6*, 774-786.

33. Sen, K. D.; Bartolotti, L. J. Density-functional-theory calculations of static dipole polarizability of some ions of interest in M\"ossbauer spectroscopy. *Phys. Rev. A* **1992,** *45*, 2076-2078.
34. Tessman, J. R.; Kahn, A. H.; Shockley, W. Electronic Polarizabilities of Ions in Crystals. *Phys. Rev.* **1953,** *92*, 890-895.
35. Vogel, P. Dipole polarizabilities from the nf term values. *Nuclear Instruments and Methods* **1973,** *110*, 241-244.